JOURNAL OF PROPULSION AND POWER
Vol. 28, No. 4, July–August 2012

Side-Force Amplification on an Aerodynamically Thrust-Vectored Aerospike Nozzle

Shannon D. Eilers,* Matthew D. Wilson,* Stephen A. Whitmore,† and Zachary W. Peterson*
Utah State University, Logan, Utah 84322

DOI: 10.2514/1.B34381

Results from cold-flow experiments on aerodynamic thrust vectoring of a small-scale annular aerospike thruster are presented. Thrust vectoring is produced by injection of a secondary fluid into the primary flowfield normal to the nozzle axis. The experimental aerospike nozzle is truncated at 57% of its full theoretical length. For these tests, carbon dioxide is the working fluid. Injection points near the end of the truncated spike produced the highest force amplification factors. Explanations are given for this phenomenon. For secondary injection near the end of the aerospike, side-force amplification factors up to 1.4, and side-force-specific impulses up to 55 s were demonstrated. By comparison, the main flow-specific impulse averaged approximately 38 s. Secondary side-injection pulses were observed to crisply reproduce side forces with a high degree of fidelity. Side-force levels approach 2.7% of the total thrust level at maximum efficiency. Higher side forces of 4.1% axial thrust were also achieved at reduced efficiency. The side-force amplification factors were independent of operating nozzle pressure ratio for the range of chamber pressures evaluated in this test series.

I. Introduction

THE aerospike nozzle differs from a conventional rocket nozzle in that the propulsive fluid expands around a plug or ramp and is not constrained by external solid boundaries as in a bell or conical nozzle. Because the external flowfield is unconstrained, the pressure on the aerospike nozzle surface has the ability to adjust to changes in ambient pressure, leading to the well-known altitude compensation effect experienced by aerospike nozzles.

A. Space Applications of Aerospike Nozzle Space

Although aerospike nozzles have long been known for their altitude-compensation ability during endo-atmospheric flight [1], they also present significant potential advantages for purely in-space applications. Aerospike nozzles can be both more efficient and significantly smaller than conventional high-expansion ratio bell nozzles. Given a fixed vehicle base area, an aerospike nozzle can present a higher area expansion ratio than a bell nozzle, providing better performance in a space environment or near-vacuum environment like Mars. The increased specific impulse (I_{sp}) due to a higher possible expansion ratio using an aerospike nozzle translates to a 8–9% decrease in the propellant mass and total system weight for space and near-space applications [2].

Figure 1 compares two aerospike-based nozzle designs with their conventional counterparts with the same effective expansion ratios [3]. Figure 1a compares the original Saturn V first-stage F-1A engine to its proposed replacement J-2T-250K aerospike engine (featuring a truncated plug nozzle). It should be noted that both of these engines are optimized for Earth atmospheric launch conditions. For vacuum conditions, the size difference is greater. This size difference is illustrated by Fig. 1b, where the proposed 12.1 kNt Altair Lander Engine is compared with its aerospike equivalent. In both examples, the size differences are pronounced.

Additionally, one of the often-overlooked properties of the aerospike nozzle is the ability to achieve thrust vectoring aerodynamically without active mechanical nozzle gimbals or differential plenum throttling. This property offers a significant potential for reduced system complexity and weight. With traditional thrust vectoring in conical or bell nozzles, the secondary injection port is far within the nozzle, making thrust vectoring without active primary flow impractical. In contrast to conventional nozzles, thrust vectoring performed by secondary injection on an aerospike nozzle could also be used for attitude control independent of main thruster operation. Aerodynamic thrust vectoring on aerospike nozzles offers a potential replacement for both gas attitude-control thrusters and main engine thrust vector gimbal control.

Despite the potential benefits of aerospike nozzles over conventional nozzle designs, because of a perceived low technology-readiness level, the aerospike configuration has never been deployed on an operational space vehicle. One of the major reasons for this perception is the lack of high-quality ground and flight test data and its correlation with analytical flow predictions. This dearth of data is especially true with regard to off-nominal design performance, thrust vectoring, and thruster-out scenarios for clustered aerospike configurations.

B. Aerospike Nozzle Development History

Significant experimentation on aerospike nozzles was first completed in the 1950s and 1960s when truncated plug nozzles were being considered for the Saturn V upper stages [4] and, later, the Space Shuttle's main engine [5–7]. During this period, Rocketdyne conducted extensive research into both aerospike performance and liquid injection thrust vectoring [8,9]. Rocketdyne concluded that aerospike nozzles had less or equal thrust vectoring capability than bell nozzle counterparts. However, their tests were limited to liquid injection. Rocketdyne did not perform cold-flow thrust-vectoring tests, and hot gas injection hardware was not yet available. After a conventional bell nozzle was chosen for the Space Shuttle main engine, work on aerospike nozzles reduced significantly until the 1990s when work began on the X-33 single stage to orbit (SSTO) vehicle [10]. Supporting this effort, significant testing was performed by Rocketdyne for Lockheed during the development of the RS-2200 linear aerospike [11–13].

After the X-33 and the Venture Star programs were canceled, aerospike nozzle development once again became sporadic. In the U.S., NASA Langley Research Center explored parametric modeling and optimization of aerospike nozzles [14]. Simultaneously, computational algorithms to evaluate thrust vector control for aerospike nozzles were developed at the University of Alabama in Huntsville [15], and differential throttling research was completed at

Presented as Paper 2011-5531 at the 47th AIAA/ASME/SAE/ASEE Joint Propulsion Conference , San Diego, CA, 28 July–3 August 2011; received 30 June 2011; revision received 21 November 2011; accepted for publication 9 February 2012.

*Graduate Research Assistant, Mechanical and Aerospace Engineering Department, 4130 Old Main Hill. Student Member AIAA.

†Associate Professor, Mechanical and Aerospace Engineering Department, 4130 Old Main Hill. Associate Fellow AIAA.

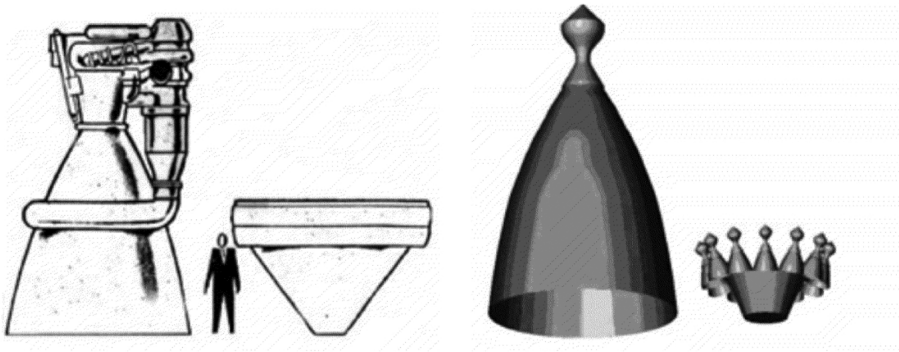

a) b)

Fig. 1 Aerospike compared with conventional nozzles. a) Comparison of F-1 engine to proposed J-2T-250 K aerospike. b) Comparison of 12.1 kNt lunar ascent engine for Altair Lander with proposed aerospike design. (Available by Special permission from JANNAF Inter-agency Propulsion Committee, Johns Hopkins University, Chemical Propulsion Information Analysis Center)

the Marshall Space Flight Center [16]. During this test series, differential throttling was found to have little effect on total nozzle efficiency, but side force was highly dependent the total nozzle pressure ratio. Engineers from NASA Dryden Flight Research Center and the U.S. Air Force Research Laboratory designed and flew an aerospike nozzle on a high-power rocket [2]. Research on adapting annular aerospike nozzles for hybrid rockets was performed at Arizona State University [17] and the University of Washington [18]. There were notable challenges due to erosion of the nozzle support structure in the former, and nozzle ablation rates were not presented in the latter. California Polytechnic University has also investigated coupling an aerospike nozzle with a hybrid rocket motor. Their efforts centered on active cooling techniques [19,20]. Their tests showed that a common hybrid oxidizer, nitrous oxide, could make an acceptable coolant fluid for aerospike nozzles. California State University, Long Beach, in association with the Garvey Spacecraft Corporation, has also completed extensive testing of liquid, clustered aerospike engines, which has culminated in the launch of several sounding rockets [21–25].

Outside of the U.S., aerospike nozzles have enjoyed a large amount of attention in recent decades. The European Space Agency has investigated the relative effectiveness of various aerospike thrust vector-control techniques [26,27]. In the mid 1990s, the Technical University of Munich performed analytical research on performance aspects of aerospike nozzles, including performance losses due to nozzle clustering [28,29]. Some research has also been completed at the German Aerospace Center, mostly concerning effects of aerospike cluster configurations [30–32]. A substantial amount of work has also been completed in Italy on performance validation, flight behavior, and motor-cluster performance for aerospike nozzles [33–37].

Significant analytical work has been performed at several universities in Japan on aerospike performance, slipstream effects, slipstream effect mitigation, and base-bleed injection [38–46]. Experimental work has also been completed in Japan to investigate the flowfield of clustered linear aerospike nozzles [47]. Conceptual design of a SSTO vehicle aerospike nozzle has been undertaken recently at the Japan Aerospace Exploration Agency [48–50]. Beijing University in China has performed analysis as well as cold-flow tests on aerospike nozzles. These tests investigated nozzle performance, base-bleed effects, and thrust vectoring [6,51–54], mostly in regard to linear aerospike engines.

The National Aerospace Laboratories in Bangalore, India, have investigated the acoustics of aerospike nozzles [55] and performance characteristics of conical aerospike nozzle contours [56]. Some analytical work has also been completed in Russia on optimal aerospike contours [57]. The Aerospace Research Institute in Iran has also completed some work on base-bleed performance [58].

Although aerospike nozzles have seen a resurgence in research attention in the past decade, little attention has been given to thrust vectoring via secondary flow addition since the initial research by Rocketdyne.

C. Gaseous Injection Development History

Thrust-vectoring effectiveness is commonly defined in terms of a ratio of either side-force-specific impulse to axial force-specific impulse or side-force-specific impulse to side-force-specific impulse without axial flow. In this paper, the side-force amplification factor is defined as the ratio of side force produced with a main axial flow (and corresponding amplifying flow effects) to the side force with secondary injection but without primary flow. This is similar to the definition used by Walker et al. [59] in thrust-vectoring research performed at Johns Hopkins University. Using this definition for the side-force amplification factor avoids the dependence on the arbitrary efficiency of the primary thruster.

Thrust-vectoring efficiency for gas injection into conical nozzles has been well established, although data for gaseous injection are not as available as that for liquid injection. Work performed by Gunter and Farenholz [60] on cold-flow tests with a conical nozzle yielded amplification factors of approximately 2.0. Walker et al. [59] also performed cold-flow tests, including some with carbon dioxide as a working fluid, and had side-force amplification factors that ranged from approximately 1.8 to 3.0, with the highest amplification factors gained by the smallest orifices. Inouye [61] performed a series of hot-gas injection tests and produced amplification factors generally between about 1.2 and 1.8 for a motor and secondary injection motor using red fuming nitric acid and unsymmetrical dimethylhydrazine.

II. Experimental Apparatus, Setup, and Test Procedure

A series of cold-flow tests were performed to examine the viability of fluidic thrust vectoring by gas injection on a truncated annular aerospike nozzle in near-optimally expanded conditions. Although the final aerospike nozzle was slightly overexpanded at the test conditions, it was not sufficiently overexpanded to change the near-surface flowfield. As the pressure and velocity distribution near the secondary injection orifice are nearly identical to the flowfield experienced by an underexpanded or optimally expanded nozzle, the thrust vectoring test results are applicable to high-altitude or in-space conditions. Research focused on the effects of injection port location on vectoring effectiveness and side-force fidelity. Side-force dependence on nozzle pressure ratio was also investigated.

A. Test Stand Description

All aerospike static tests were performed in the Engineering Technology Department's jet engine test cell on the Utah State University campus. For static thrust tests, commercially available test stands were examined and found to be excessively expensive and to have structural support mechanisms that were unsuitable for mounting the aerospike prototype. Consequently, a custom-made, portable test stand was designed and built to support the needs of the aerospike project.

The test stand features a 6 deg-of-freedom load balance with type S load cells configured as shown in Fig. 2. Three 100-lbf-range (445 N)

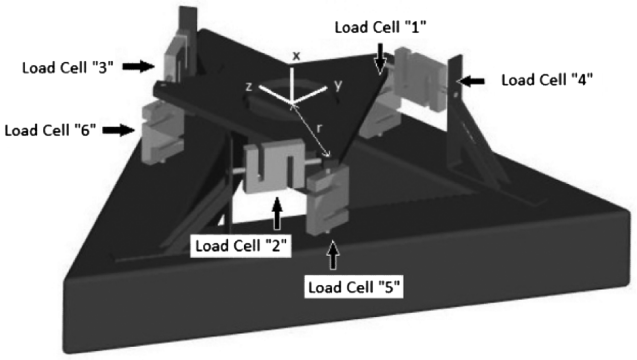

Fig. 2 6-deg-of-freedom test stand.

axial and three 25-lbf-range (111 N) lateral load cells are arranged such that 6-deg-of-freedom force and moment measurements can be resolved. The thrust stand is designed so that the nozzle exhaust plume exits vertically, and the thrust acts downward onto the test cart. The thrust stand coordinate system, also pictured in Fig. 2, is defined with the x axis aligned vertically upward along the axial centerline of the nozzle. The test stand was calibrated in situ with a simultaneously multi-axial calibration method. The total resultant uncertainty (to 95% confidence) for forces using this calibration method was statistically determined as approximately 0.25 N for side forces and 1.75 N for axial loading with nominal values of 15 N and approximately 400 N, respectively [62].

For ease of storage and handling, carbon dioxide was chosen for a working fluid. Figure 3 presents a plumbing and instrumentation diagram of the associated cold-gas feed system. Saturated liquid carbon dioxide is stored in standard K-sized storage tanks, with each tank having a storage capacity of approximately 25 kg. Multiple tanks were manifolded to ensure that the required mass flow levels and run times can be achieved. Flow out of the tanks is controlled via a pneumatic ball valve. The pneumatic valve actuator is controlled with a 12 V direct current solenoid valve. Beyond the ball valve, carbon dioxide flows through a manually set needle valve that drops the pressure from the saturation pressure of carbon dioxide, 4825–5515 kPa (700–800 psia) at room temperature, to approximately 1035 kPa (150 psi). Carbon dioxide then flows into a water-bath heat exchanger, which raises the temperature of the expanded carbon dioxide by approximately 25°C. The pressure downstream of the needle valve is controlled using a backflow pressure regulator and a primary regulator in parallel. The needle valve and the backflow regulator maintain approximately 1034 kPa (150 psi) upstream of the primary regulator. The primary flow regulator further drops the feed pressure to approximately 690 kPa (100 psi) at the plenum inlet.

At full pressure, the primary regulator is set to allow approximately 1 kg/s mass flow through the aerospike nozzle throat. The backpressure regulator will vent approximately half that flow rate at startup. As the tanks evacuate and the overall system pressure drops, flow through the backpressure regulator diminishes to zero. An additional electronic regulator in parallel with the main flow regulator controls the upstream pressure of the secondary (thrust vectoring and base-bleed) flow injection ports.

Type-K thermocouples and pressure transducers are used to monitor temperatures and pressures throughout the flow system. A custom-manufactured Venturi flow meter, also using pressure transducers to measure the pressure differential, is situated upstream of the electronic regulator. Although a differential pressure transducer was not used, the pressure transducer voltage bias is removed at full operating pressure when the secondary flow injection is turned fully off. This results in a differential pressure measurement accurate to within about 0.1% of differential reading. The Venturi was calibrated in situ using high flow coefficient sonic orifices. In this manner, the flow coefficient for the Venturi was calculated to be 0.980, which is very near the expected result for Venturi flow meters of this design. The typical mass flow rate uncertainty with this Venturi was about 1.0% of the measurement.

B. Test Article Description

Because of manufacturing considerations (high expansion ratios yield larger aerospike nozzles, which are easier to manufacture), the aerospike nozzle used for cold-flow experimentation is sized to be slightly overexpanded for operating conditions at the test altitude, 1450 m (about 86.2 kPa), in Logan, Utah. The resulting expansion ratio is 2.47. It is desirable to keep the near-surface flowfield close to what would be experienced in in-space or underexpanded conditions. To accomplish this, the aerospike was designed using a method of characteristics code to verify that compression waves generated by overexpansion would not intersect the end of the truncated spike at full chamber pressure. The resulting plug was truncated such that the test article was 57% of the length of a full spike. This design results in an aerospike pressure distribution roughly independent of atmospheric pressure, except for the base area and the very end of the spike length. This effect was confirmed through the use of computational fluid dynamics. The salient aerospike characteristics are shown in Table 1, and the aerospike and plenum geometries are shown in Figs. 4 and 5.

III. Experimental Results

Aerospike nozzle configurations with secondary injection ports located at 20, 80, and 90% axial position along the truncated spike were tested with secondary mass flow rates between 0.005 and 0.016 kg/s and primary mass flow rates between 0.70 and 0.95 kg/s. These flow rates correspond to secondary flow inlet

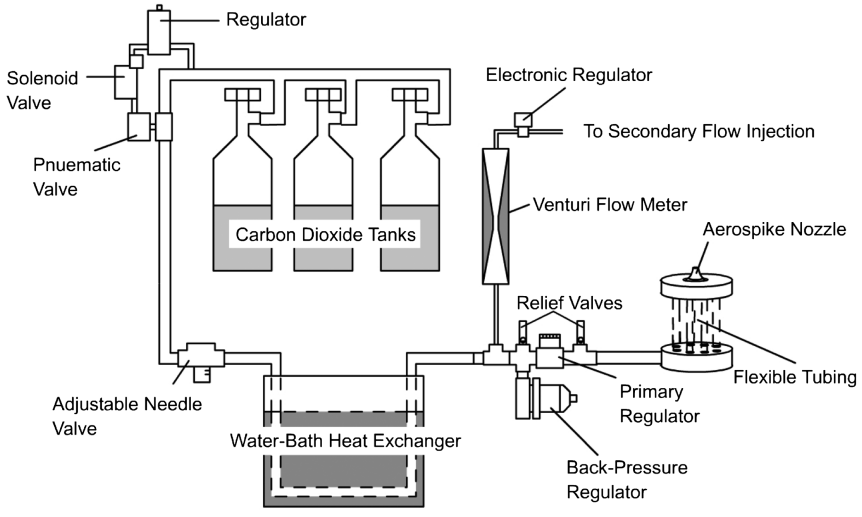

Fig. 3 Aerospike propellant feed system.

Table 1 Cold-flow aerospike parameters

Aerospike Parameter	Value
Plug diameter	3.2 cm
Outer throat diameter	3.86 cm
Truncated length	2.54 cm
Full isentropic spike length	4.31 cm
Truncation ratio	57%
Throat diameter	0.29 cm
Operating stagnation pressure	775 kPa
Nozzle expansion ratio	2.47
Plenum exit throat area	4.73 cm^3
Secondary injection port diameter	0.3175 cm
Design altitude	4206 m MSL
Design thrust	454 N
Design mass flow rate	1.0 kg/s

pressures between approximately 400 and 800 kPa and primary plenum pressures between about 350 and 600 kPa. The secondary injection orifices were machined such that they injected fluid normal to the aerospike's longitudinal axis. These port locations are shown in Fig. 4. Lateral force, secondary injection pressure, mass flow rate, and temperatures for two typical tests are shown in Fig. 6. The side force, specific impulse, and secondary flow pressure for the 90% secondary injection location for both main flow on and main flow off is shown in Fig. 7. The response fidelity between the electronic regulator control and the output size force is clearly shown in both of these figures. A high degree of repeatability and crisp thrust vectoring response was typical of the entire test series.

The resulting side-force amplification factor and specific impulse for each configuration is shown in Table 2 and Fig. 8. An additional configuration with a larger-diameter injection orifice and at approximately 90% the length of the truncated spike was also tested to examine side-force scaling. These results are shown in Fig. 9.

The use of carbon dioxide as a operating fluid allowed for excellent test flow visualization when the fluid crystallizes near the end of the aerospike contour. This phase change creates a semi-opaque cloud that is readily visible. The temperature increase caused by shock waves resulting from secondary fluid injection creates clear areas in the flowfield that are easily distinguishable. The leading edge bow shock caused by fluid injection for a high flow rate test is clearly seen in Fig. 10.

During the cold-flow test series, the ratio of the chamber pressure to ambient pressure was varied from approximately 5.0 to 8.0. No meaningful correlation between side-force-specific impulse and chamber pressure was observed over this range. The side force I_{sp} for this range with the 90% injection orifice location is shown in Fig. 11. Near the upper part of this range, the nozzle surface pressure is effectively independent of ambient pressure. At lower pressure ratios, aerospike altitude compensation influences local ambient Mach number and density around the secondary flow orifice. It is probable that the variation of these two parameters has counterbalancing influences on the side-force-specific impulse over the range of pressure ratios examined during cold-flow testing.

It is notable that the secondary injectant does not reach sonic velocity at the immediate exit of the injection orifice. The bow shock caused by primary flow results in an effectively reduced orifice exit area for the injectant immediately downstream of the orifice. This reduced area results in a drop in discharge coefficient of approximately 5% between tests with secondary injection only and secondary injection with active primary flow.

For aerospike configurations with the secondary injection point near the end of the aerospike, the effect of secondary fluid injection on axial thrust was small enough such that it was not detectable by the current testing apparatus. The maximum side force for the larger orifice is approximately 14 N. For these tests, the average primary thrust level is 343 N. This results in a total thrust vector deflection of about 2.3 deg or a side-force level of 4.1%. Resultant cosine losses for this thrust angle are therefore less than 0.1%, so it is not surprising that no net effect on axial thrust is detected at these side-force levels. Similarly, maximum side-force levels for the smaller, more efficient orifice size were about 8 N. This yields a net side-force level of about 2.3% or about 1.3 deg. Cosine losses for this configuration would be on the order of 0.03%.

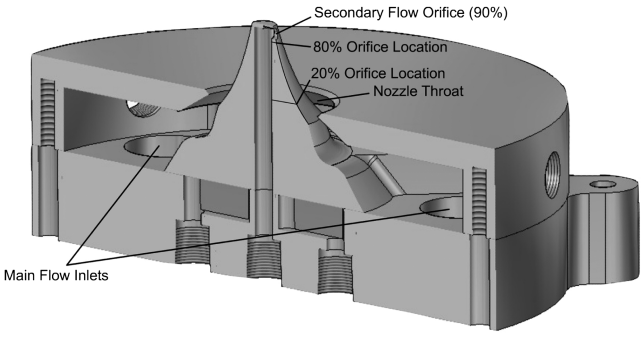

Fig. 4 Cold-flow aerospike test configuration.

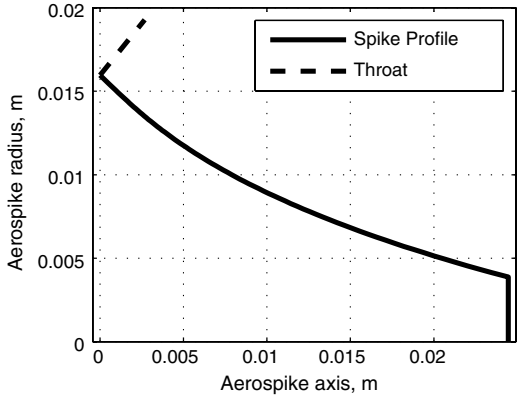

Fig. 5 Cold-flow aerospike profile.

IV. Effect of Longitudinal Injection Location

The test series showed a marked dependence for side-force amplification factor on longitudinal hole location. Over the range of locations examined in this test series, the optimal injection location was at the aft edge of the truncated aerospike length. This is clearly shown in Fig. 12. This trend is in direct contradiction to side-force relations historically obtained on conical nozzles. For lab scale tests on conical nozzles, the optimum injection point for gas injection has been found to be nearest the throat where the resulting bow shock does not impinge on the opposite nozzle wall [60]. Two explanations for this optimal port location are diminishing the effect of the low pressure, overexpanded region directly downstream of the injection location and the effect of local primary flow Mach number at the injection location.

The mechanism for side-force generation by secondary injection on an aerospike nozzle differs significantly from those generated by side injection on a conventional nozzle. Figure 13 compares the side-injection flow patterns on conventional and aerospike nozzles. In both cases, the injected flow produces a strong shock wave and a significant proverse pressure increase behind the shock wave. In both cases, there is also a low-pressure region caused by overexpansion of the secondary injectant into the primary flowfield. These flow regions have been amply studied during secondary injection experiments completed on flat plates [63,64]. In a conventional nozzle, the flow aft of this injection point follows a concave path away from the centerline. This limits the deterioration of the high-pressure region caused by the shock wave as the entire shock wave is captured by the nozzle geometry. Thus, the effects of the leading shock wave and the low pressure region due to overexpansion tend to cancel out in a bell nozzle [65,66].

On an aerospike nozzle, however, the flow behind the injection point follows a convex path. Directly downstream of the injection site

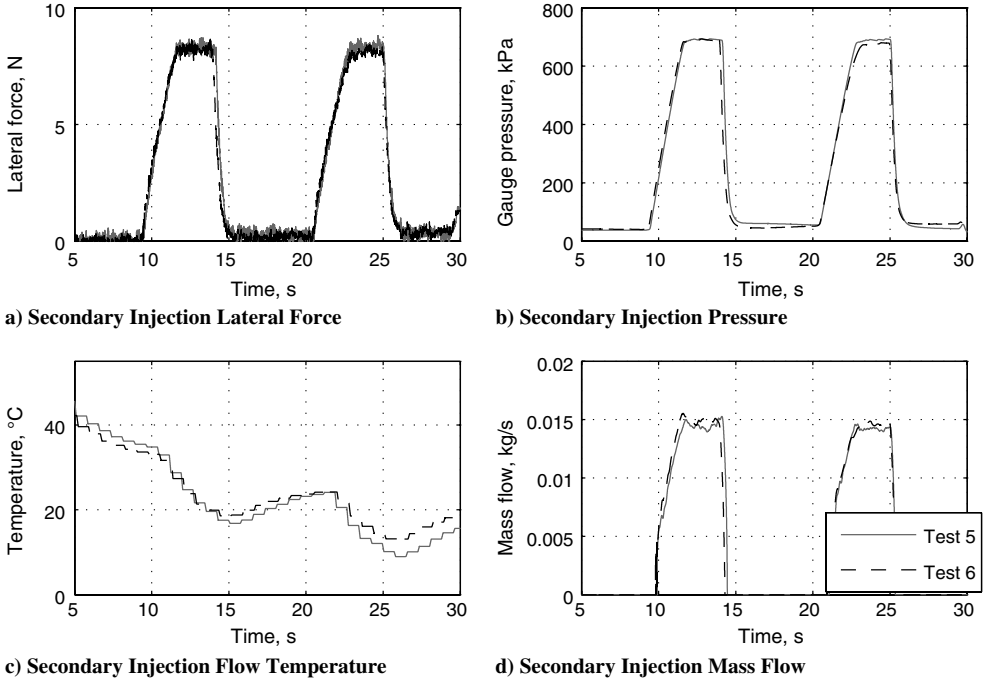

a) Secondary Injection Lateral Force

b) Secondary Injection Pressure

c) Secondary Injection Flow Temperature

d) Secondary Injection Mass Flow

Fig. 6 Side force and secondary injection pressure for 90% injection point.

there occurs a predicted drop in Mach number and a corresponding pressure increase. Because of the convex aerospike nozzle shape, the secondary injection disturbance propagates across the entire upper spike surface downstream of the injection site, and the convex surface contour results in a flow expansion on the injectant side of the nozzle. When the injection occurs on the upstream portions of the nozzle, the resulting expansion region offsets any gain achieved by the high-pressure compression behind the shock wave. The net result is a total side force that is less than what would be produced by the injected pulse alone.

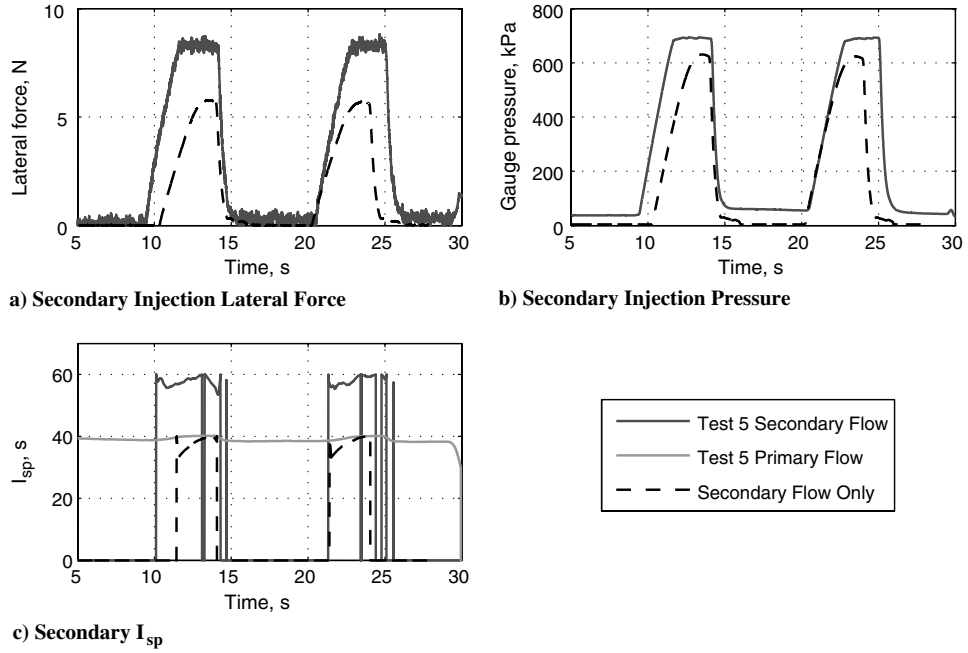

a) Secondary Injection Lateral Force

b) Secondary Injection Pressure

c) Secondary I_{sp}

Fig. 7 Side force and secondary injection for 90% injection point for both primary-flow-only and secondary-flow-only configurations.

Table 2 Cold-flow test specific-impulse results

Test series	I_{sp}, s	I_{sp} uncertainty, s, 95%	Amplification factor
Injection location at 90%	54.8	±1.9	1.39
Injection location at 80%	47.0	±1.9	1.19
Injection location at 20%	21.2	±1.7	0.54
Secondary flow only	39.5	±1.8	

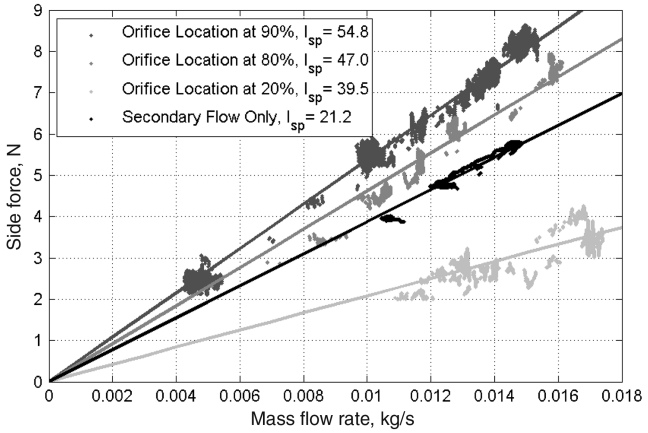

Fig. 8 Cold-flow secondary injection results and regressed specific impulses for various hole locations.

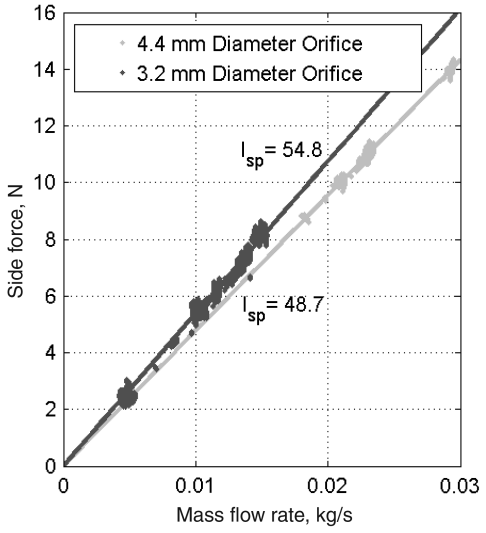

Fig. 9 Cold-flow secondary injection with increased secondary orifice diameter results.

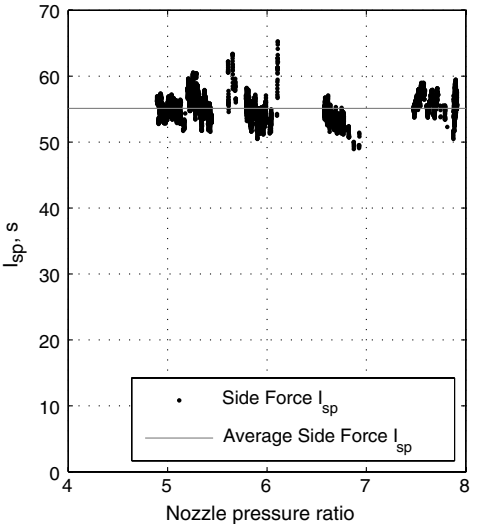

Fig. 11 Cold-flow specific impulse vs nozzle pressure ratio.

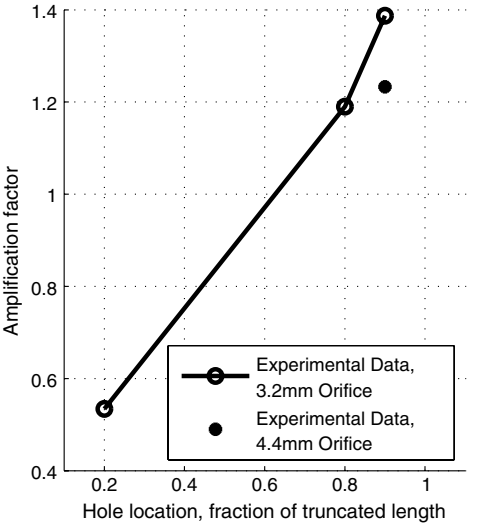

Fig. 12 Cold-flow specific impulse vs secondary injection location.

When the injection location is near the end of the aerospike, the effect of the low-pressure region is diminished, which results in large efficiency gains. As the aerospike flow is sufficiently expanded such that the base of the aerospike feels atmospheric pressure, the secondary injection entrains flow from the base region without causing a significant reduction in base pressure. This drives a complex flowfield of counter rotating vortexes that drag fluid from the separated base towards the secondary injection jet. This fluid flow keeps the secondary flow from significantly overexpanding after the

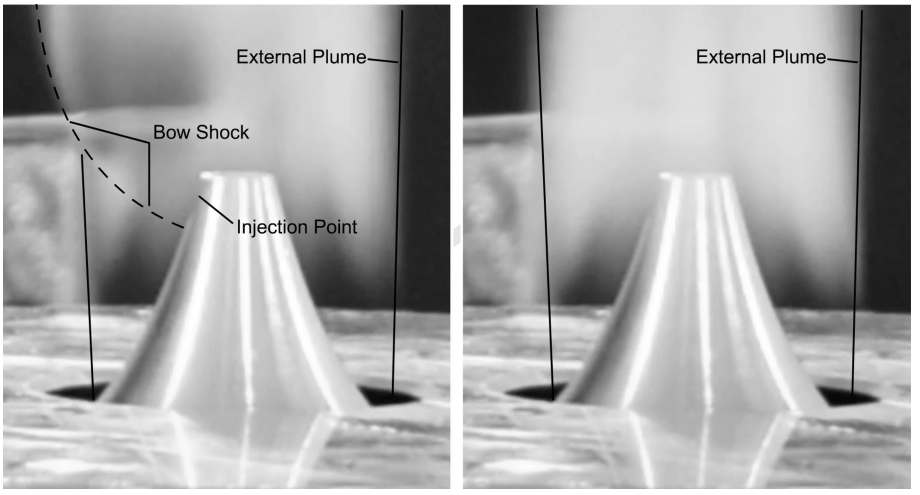

Fig. 10 Aerospike cold-flow test with 4.4 mm diameter orifice located at 90% of the length of the truncated aerospike. a) Thrust vectoring on, showing clear bow shock. b) Thrust vectoring off.

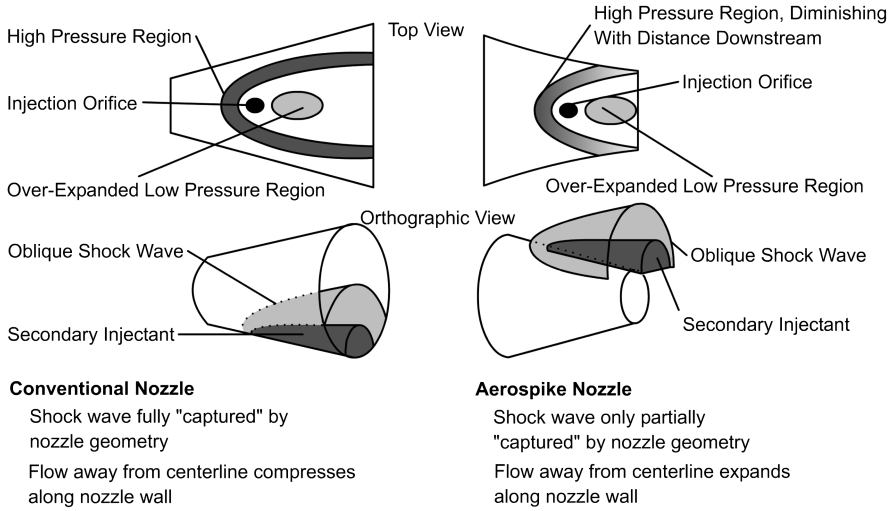

Fig. 13 Representative side-injection flow patterns on conventional and aerospike nozzles.

secondary injection orifice, increasing the thrust vectoring efficiency. As the aerospike is operating in open wake conditions where the aerospike base adjusts to ambient pressure, this does not adversely impact thrust in the longitudinal direction. Future computational and/or experimental results will be required to examine if thruster efficiency in the primary direction is at all compromised in low-ambient-pressure or closed-wake conditions when the aerospike base is independent of ambient pressure.

V. Conclusions

Fluidic thrust vectoring on a truncated aerospike nozzle was performed with carbon dioxide as a working fluid. A marked dependence of thrust-vectoring efficiency on longitudinal orifice location was discovered. To enhance the thrust vectoring effectiveness of side-force injection on a three-dimensional aerospike nozzle, the injection site must be moved aft so that flow over-expansion does not occur on the surface of the physical spike. This assertion is in direct contrast to what was previously known about side injection on conventional nozzles. Data were collected for configurations with side-injection port locations at 20, 80, and 90% of the nozzle length; and significant force amplification factors were observed for orifices near the end of the nozzle. The side-force-specific impulse at the 90% port location is enhanced by nearly 40%. The enhanced side force I_{sp} means that the same control impulse can be achieved for significantly less propellant than would be used by a stand-alone reaction control thruster.

Although the amplification factors generated for the cold-flow aerospike in this test are somewhat lower than for conical nozzles, it should be noted at all of the conical nozzle test series described in this paper involved a much higher primary flow pressure ratio than those examined in the cold-flow aerospike tests for this test series. Additionally, the high-end amplification factors generated for conical nozzles generally corresponded to very small secondary orifice diameters. It is expected that variation of orifice size on an aerospike nozzle would likewise show a maximum at some orifice diameter.

Because of the ability to use thrust-vectoring ports on an aerospike nozzle for small impulse attitude control maneuvers without primary flow active, it also provides the possibility to replace conventional reaction control thrusters.

The primary gain from thrust vectoring on an aerospike nozzle is the ability to use secondary injection jets as stand-alone reaction control without the use of the primary engine. When the primary thruster is fired, then the additional benefits of flow amplification are gained. A jet internal to a conventional nozzle would obviously not share this same operational advantage. This, coupled with the volumetric efficiency gains of aerospike nozzles, makes aerospike nozzles with thrust vectoring a strong option for small satellite missions.

References

[1] Ruf, J. H., and McConnaughey, P. K., "The Plume Physics Behind Aerospike Nozzle Altitude Compensation and Slipstream Effect," *33rd AIAA/ASME/SAE/ASEE Joint Propulsion Conference & Exhibit*, AIAA 1997-3217, Seattle, WA, 1997.

[2] Bui, T., Murray, J., Rogers, C., Bartel, S., Cesaroni, A., and Dennett, M., "Flight Research of an Aerospike Nozzle Using High Power Solid Rockets," *41st AIAA/ASME/SAE/ASEE Joint Propulsion Conference & Exhibit*, AIAA 2005-3797, Tucson, AZ, 2005.

[3] Mungas, G. S., Fisher, D. J., Johnson, M., and Rishikof, B., "NOFB Monopropulsion System for Lunar Ascent Vehicle Utilizing Plug Nozzle Ascent Engine". *Joint Army, Navy, NASA, Air Force Interagency Propulsion Conference*, NASA LPS-II-33, Colombia, MD, Dec. 2008.

[4] "Final Report—Studies of Improved Saturn V Vehicles and Intermediate Payload Vehicles," The Boeing Company TR D5-13183, 1966.

[5] Bendersky, C., *Space Shuttle Propulsion Issue: Staged Combustion Bell Versus Tap-Off or Gas-Generator Aerospike*, Bellcomm, Inc. TM 70-1013-1, 1970.

[6] Berman, K., and Crimp, F. W., Jr., "Performance of Plug-Type Rocket Exhaust Nozzles," *ARS Journal*, Vol. 31, No. 1, 1961, pp. 18–23.

[7] Hendershot, K. C., Sergeant, R. J., and Wilson, H. B., "A New Approach for Evaluating the Performance and Base Environment Characteristics of Nonconventional Rocket Propulsion Systems," AIAA Paper 1967-256, 1967.

[8] "Final Report, Advanced Aerodynamic Spike Configurations, Volume 1," AFRPL TR 67-246, Vol. 1, 1967.

[9] "Final Report, Advanced Aerodynamic Spike Configurations, Volume 2," AFRPL TR. 67-246, Vol. 2, 1967.

[10] Korte, J. J., Salas, A. O., Dunn, H. J., Alexandrov, N. M., Follett, W. W., Orient, G. E., and Hadid, A. H., "Multidisciplinary Approach to Aerospike Nozzle Design," NASA TM 110326, 1997.

[11] Booth, T., Vilja, J. O., Cap, D. P., and McGill, R. J., "The Design of Linear Aerospike Thrust Cells," AIAA Paper 1993-2562, 1993.

[12] Erickson, C., "Thrust Vector Control Selection in Aerospike Engines," *AIAA Journal*, Vol. 97, No. 3307, 1997, pp. 1–6.

[13] Heald, D. A., and Hart, D. A., "Advanced Reusable Engine for SSTO," *27th AIAA/SAE/ASME Joint Propulsion Conference*, AIAA 1991-2181, Sacramento, CA, 1991.

[14] Korte, J. J., "Parametric Model of an Aerospike Rocket Engine," AIAA 2000-1044, 2000.

[15] Higdon, K., and Landrum, D. B., "Analysis of Annular Plug Nozzle Performance and TVC," AIAA Paper 2003-4908, 2003.

[16] Ruf, J., and McDaniels, D., "Experimental Results for an Annular Aerospike with Differential Throttling," *5th International Symposium on Liquid Space Propulsion*, NASA TM 0217125, 2003.

[17] Shark, S. C., Dennis, J. D., and Villarreal, J. K., "Experimental Performance Analysis of a Toroidal Aerospike Nozzle Integrated with a

N2O/HTPB Hybrid Rocket Motor," *46th AIAA/ASME/SAE/ASEE Joint Propulsion Conference & Exhibit*, AIAA 2010-6784, Nashville, TN, 2010.

[18] Stoffel, J. R., "Experimental and Theoretical Investigation of Aerospike Nozzles in a Hybrid Rocket Propulsion System," *47th AIAA Aerospace Sciences Meeting*, AIAA 2009-219, Orlando, FL, 2009.

[19] Lemieux, P., "Development of a Reusable Aerospike Nozzle for Hybrid Rocket Motors," *39th AIAA Fluid Dynamics Conference*, AIAA 2009-3720, San Antonio, TX, 2009.

[20] Lemieux, P., "Nitrous Oxide Cooling in Hybrid Rocket Nozzles," *Progress in Aerospace Sciences*, Vol. 46, 2010, pp. 106–115. doi:10.1016/j.paerosci.2009.12.001

[21] Ladeinde, T., and Chen, H., "Performance Comparison of a Full-Length and a Truncated Aerospike Nozzle," *46th AIAA/ASME/SAE/ASEE Joint Propulsion Conference & Exhibit*, AIAA 2010-6593, Nashville, TN, 2010.

[22] Wilson, A., Clark, J., Besnard, E., and Baker, M., "CFD Analysis of a Multi-Chamber Aerospike Engine in Over-Expanded, Slipstream Conditions," *45th AIAA/ASME/SAE/ASEE Joint Propulsion Conference & Exhibit*, AIAA 2009-5486, Denver, CO, 2009.

[23] Besnard, E., and Garvey, J., "Aerospike Engines for Nanosat and Small Launch Vehicles (NLV/SLV)," *AIAA Space 2004 Conference and Exhibit* AIAA Paper 2004-6005, San Diego, CA, 2004.

[24] Besnard, E., and Garvey, J., "Development and Flight-Testing of Liquid Propellant Aerospike Engines," *40th AIAA/ASME/SAE/ASEE Joint Propulsion Conference and Exhibit*, AIAA 2004-3354, Fort Lauderdale, FL, 2004.

[25] Chang-Hui, W., Liu, Y., and Qin, L.-Z., "Aerospike Nozzle Contour Design and its Performance Validation," *Acta Astronautica*, Vol. 64, 2009, pp. 1264–1275. doi:10.1016/j.actaastro.2008.01.045

[26] Schoyer, H. F. R., "Thrust Vector Control for (Clustered Modules) Plug Nozzles: Some Considerations," *Journal of Propulsion and Power*, Vol. 16, 2000, pp. 196–201. doi:10.2514/2.5583

[27] Hallard, R., and Merienne, M. C., "Aerospike Nozzle Tests," *Proceedings of the Third European Symposium on Aerodynamics for Space Vehicles*, Vol. 426, European Space Agency, Noordwijk, The Netherlands, 1998, pp. 387–394.

[28] Fick, M., "Performance Modeling and Systems Aspects of Plug Cluster Nozzles," *34th AIAA/ASME/SAE/ASEE Joint Propulsion Conference & Exhibit*, AIAA 1998-3525, Cleveland, OH, 1998.

[29] Fick, M., and Schmucker, R. H., "Remarks on Plug Cluster Nozzles," *31st AIAA/ASME/SAE/ASEE Joint Propulsion Conference and Exhibit*, AIAA Paper 1995-2694, San Diego, CA, 1995.

[30] Hagemann, G., Schley, C.-A., Odintsov, E., and Sobatchkine, A., "Nozzle Flowfield Analyses With Particular Regard to 3-D-Plug Cluster Configurations," AIAA Paper 1996-2954, 1996.

[31] Hagemann, G., Immich, H., Nguyen, V., and Dumnov, G., "Advanced Rocket Nozzles," *Journal of Propulsion and Power*, Vol. 14, No. 5, Sept.–Oct. 1998, pp. 620–634. doi:10.2514/2.5354

[32] Rommel, T., Hagemann, G., Schley, C., Manski, D., and Krulle, G., "Plug Nozzle Flowfield Calculations for SSTO Applications," *31st AIAA/ASME/SAE/ASEE Joint Propulsion Conference and Exhibit*, AIAA Paper 1995-2784, San Diego, CA, 1995.

[33] Sorge, R., Carmicino, C., and Nocito, A., "Design of a Lab-Scale Cooled Two-Dimensional Plug Nozzle for Experimental Tests," *38th AIAA/ASME/SAE/ASEE Joint Propulsion Conference & Exhibit*, AIAA 2002-4039, Indianapolis, IN, 2002.

[34] Nasuti, F., Geron, M., and Paciorri, R., "Three Dimensional Features of Clustered Plug Nozzle Flows," *39th AIAA/ASME/SAE/ASEE Joint Propulsion Conference & Exhibit*, AIAA 2003-4910, Rome, Italy, 2003.

[35] Nasuti, F., and Onofri, M., "Analysis of In-Flight Behavior of Truncated Plug Nozzles," *36th AIAA/ASME/SAE/ASEE Joint Propulsion Conference & Exhibit*, AIAA 2000-3289, Huntsville, AL, 2000.

[36] Onofri, M., and Nasuti, F., "Prediction of Open and Closed Wake in Plug Nozzles," *The 4th European Symposium for Aerothermodynamics for Space Applications*, European Space Agency SP-487, Capua, Italy, 2002.

[37] Onofri, M., "Plug Nozzles: Summary of Flow Features and Engine Performance," *AIAA Journal*, Vol. 1, No. 007, 2002, pp. 1–26.

[38] Fujii, K., Imai, K., and Sato, T., "Computational Analysis of the Flow Field Near the Boat-Tail Region of Annular Plug Nozzles," *JSME International Journal*, Vol. 45, 2002, pp. 745–751. doi:10.1299/jsmeb.45.745

[39] Ito, T., and Fujii, K., "Flow Field and Performance Analysis of an Annular-Type Aerospike Nozzle with Base Bleeding," *Transactions of the Japan Society for Aeronautical and Space Sciences*, Vol. 46, No. 151, 2003, pp. 17–23. doi:10.2322/tjsass.46.17

[40] Ito, T., and Fujii, K., "Numerical Analysis of the Base Bleed Effect on the Aerospike Nozzles," *Transactions of the Japan Society for Aeronautical and Space Sciences*, Vol. 46, No. 151, 2003, pp. 17–23. doi:10.2322/tjsass.46.17

[41] Ito, T., and Fujii, K., "Flow Field Analysis of the Base Region of Axisymmetric Aerospike Nozzles," *39th AIAA Aerospace Sciences Meeting & Exhibit*, AIAA Paper 2001-1051, 2001.

[42] Ito, T., Fujii, K., and Hagemann, G., "Numerical Investigation of the Side-Fence Effect on Linear Plug Nozzle Performance," AIAA Paper 2004-4018, 2004.

[43] Ito, T., Fujii, K., and Hayashi, A., "Computations of the Axisymmetric Plug Nozzle Flow Fields: Flow Structures and Thrust Performance," *17th AIAA Applied Aerodynamics Conference*, AIAA Paper 1999-3211, 1999.

[44] Miyamoto, H., Matsuo, A., and Kojima, T., "Effects of Sidewall Configurations on Rectangular Plug Nozzle Performance," AIAA Paper 2006-4373, 2006.

[45] Negishi, H., and Fujii, K., "Computational Analysis of the Effective Secondary-Flow Injections for the Plug-Nozzle Drag Reduction," *33rd AIAA Fluid Dynamics Conference and Exhibit*, AIAA 2003-3921, Orlando, FL, 2003.

[46] Tsutsumi, S., Yamaguchi, K., Teramoto, S., and Nagashima, T., "Clustering Effects on Performance and Heating of Linear Aerospike Nozzle," *45th AIAA Aerospace Sciences Meeting & Exhibit*, AIAA 2007-0122, Reno, NV, 2007.

[47] Taniguchi, M., Mori, H., Nishihira, R., and Niimi, T., "Experimental Analyses of Flow Field Structures around Clustered Linear Aerospike Nozzles," *American Institute of Physics Conference Proceedings*, Vol. 762, American Institute of Physics, Bari, Italy, 2005, pp. 349–354.

[48] Tomita, T., Takahashi, M., Onodera, T., and Tamura, H., "A Simple Performance Prediction Model of Clustered Linear Aerospike Nozzles," *37th AIAA/ASME/SAE/ASEE Joint Propulsion Conference & Exhibit*, AIAA 2001-3560, Salt Lake City, UT, 2001.

[49] Tomita, T., Kumada, N., and Ogiwara, A., "A Conceptual System Design for a Linear Aerospike Engine Applied to a Future SSTO Vehicle," *46th AIAA/ASME/SAE/ASEE Joint Propulsion Conference & Exhibit*, AIAA 2010-7060, 2010.

[50] Tomita, T., Takahashi, M., Onodera, T., and Tamura, H., "Effects of Base Bleed on Thrust Performance of a Linear Aerospike Nozzle," *35th AIAA/ASME/SAE/ASEE Joint Propulsion Conference and Exhibit*, AIAA Paper 1999-2586, 1999.

[51] Chun-Guang, J., Yu, L., Chang-Hui, W., Wen-Bo, X., and Zhen, L., "A Study for Thrust Vector Control of Aerospike Nozzle Based on Second Injection," *Journal of Propulsion Technology*, Vol. 30, No. 1, 2009, pp. 66–71.

[52] Spring, J., Xiao, P., Yu, L., and Yunfei, L., "Plug Nozzle Thrust Vector Control Study," *Technological Sciences*, Vol. 3, 2009, pp. 505–510.

[53] Li, J., Liu, Y., Liao, Y., Wang, C., Wang, Y., and Wang, N., "Experimental and Numerical Study on Two Dimensional Plug Nozzle," *46th AIAA/ASME/SAE/ASEE Joint Propulsion Conference & Exhibit*, AIAA 2010-6659, Nashville, TN, 2010.

[54] Yu, L., Wuye, D., Zhengke, Z., Lizi, Q., and Yibai, W., "Numerical Investigation on Linear Aerospike Nozzles," *37th AIAA/ASME/SAE/ASEE Joint Propulsion Conference and Exhibit*, AIAA 2001-3568, Salt Lake City, UT, 2001.

[55] Karthikeyan, N., Verma, S. B., and Venkatakrishnan, L. V., "Experimental Investigation of the Acoustics of an Annular Aerospike Nozzle Flow," *15th AIAA/CEAS Aeroacoustics Conference*, AIAA 2009-3375, Miami, FL, 2009.

[56] Verma, S. B., "Performance Characteristics of an Annular Conical Aerospike Nozzle with Freestream Effect," *44th AIAA/ASME/SAE/ASEE Joint Propulsion Conference & Exhibit*, AIAA 2009-5290, Hartford, CT, 2008.

[57] Kraiko, A. N., and Tillyayeva, N. I., "Contouring Spike Nozzles and Determining the Optimal Direction of their Primary Flows," *Fluid Dynamics*, Vol. 42, No. 2, 2007, pp. 321–329. doi:10.1134/S0015462807020172

[58] Naghib-Lahouti, A., and Tolouei, E., "Investigation of the Effect of Base Bleed on Thrust Performance of a Truncated Aerospike Nozzle In Off-Design Conditions," *European Conference on Computational Fluid Dynamics*, ECCOMAS, Delft, The Netherlands, 2006.

[59] Walker, P. E., Stone, A. R., and Shander, M., "Secondary Gas Injection in a Conical Rocket Nozzle: Effect of Orifice Diameter and Molecular Weight of Injectant," The Johns Hopkins Univ. Applied Physics Lab. CM-1010, 1962.

[60] Gunter, F. L., and Farenholz, F. E., "Final Report on a Study of Rocket

Thrust Control by Gas Injection," Massachusetts Inst. of Technology Naval Supersonic Laboratory TR 448, 1961.

[61] Inoyue, T., "Experiments on Rocket Thrust Vector Control by Hot Gas Injection," *Journal of Spacecraft and Rockets*, Vol. 3, No. 5, 1966, pp. 737–739. doi:10.2514/3.28522

[62] Eilers, S. D., Wilson, M. D., and Whitmore, S. A., "Analytical and Experiment Evaluation of Aerodymamic Thrust Vectoring on an Aerospike Nozzle," *46th AIAA/ASME/SAE/ASEE Joint Propulsion Conference & Exhibit*, AIAA 2010-6964, 2010.

[63] Zukoski, E. E., and Spaid, F. W., "Secondary Injection of Gases into a Supersonic Flow," *AIAA Journal*, Vol. 2, No. 10, 1964, pp. 1689–1697. doi:10.2514/3.2653

[64] Guhse, R. D., "On Secondary Gas Injection in Supersonic Nozzles," *Journal of Spacecraft and Rockets*, Vol. 3, No. 1, 1966, pp. 143–149.

[65] Wu, J.-M., Chapkins, R. L., and Mager, A., "Approximate Analyses of Thrust Vector Control by Fluid Injection," *ARS Journal*, Vol. 31, No. 12, 1961, pp. 1677–1684.

[66] Besnard, E., Chen, H. H., and Mueller, T., "Design, Manufacturing and Test of a Plug Nozzle Rocket Engine," AIAA Paper 2002-4038, 2002.

C. Segal
Associate Editor